Scaling and anisotropy in magnetohydrodynamic turbulence in a strong mean magnetic field

Roland Grappin, Wolf-Christian Müller

▶ **To cite this version:**

Roland Grappin, Wolf-Christian Müller. Scaling and anisotropy in magnetohydrodynamic turbulence in a strong mean magnetic field. Physical Review E , 2010, 82 (2), pp.26406. 10.1103/PhysRevE.82.026406 . hal-01553775

HAL Id: hal-01553775
https://hal.science/hal-01553775v1

Submitted on 10 Mar 2022

HAL is a multi-disciplinary open access archive for the deposit and dissemination of scientific research documents, whether they are published or not. The documents may come from teaching and research institutions in France or abroad, or from public or private research centers.

L'archive ouverte pluridisciplinaire **HAL**, est destinée au dépôt et à la diffusion de documents scientifiques de niveau recherche, publiés ou non, émanant des établissements d'enseignement et de recherche français ou étrangers, des laboratoires publics ou privés.

Scaling and anisotropy in magnetohydrodynamic turbulence in a strong mean magnetic field

Roland Grappin[1,2,*] and Wolf-Christian Müller[3,†]
[1]*LUTH, Observatoire de Paris, 5 Place Janssen, F-92915 Meudon, France*
[2]*LPP, Ecole Polytechnique, 91 Palaiseau, France*
[3]*Max-Planck Institut für Plasmaphysik, 85748 Garching, Germany*
(Received 31 July 2009; revised manuscript received 29 July 2010; published 20 August 2010)

We present an analysis of the anisotropic spectral energy distribution in incompressible magnetohydrodynamic turbulence permeated by a strong mean magnetic field. The turbulent flow is generated by high-resolution pseudospectral direct numerical simulations with large-scale isotropic forcing. Examining the radial energy distribution for various angles θ with respect to $\mathbf{B}_0$ reveals a specific structure which remains hidden when not taking axial symmetry with respect to B_0 into account. For each direction, starting at the forced large scales, the spectrum first exhibits an amplitude drop around a wave number k_0 which marks the start of a scaling range and goes on up to a dissipative wave number $k_d(\theta)$. The three-dimensional spectrum for $k \geq k_0$ is described by a single θ-independent functional form $F(k/k_d)$, with the scaling law being the same in every direction. The previous properties still hold when increasing the mean field from $B_0=5$ up to $B_0=10b_{\mathrm{rms}}$, as well as when passing from resistive to ideal flows. We conjecture that at fixed B_0 the direction-independent scaling regime is reached when increasing the Reynolds number above a threshold which raises with increasing B_0. Below that threshold critically balanced turbulence is expected.

DOI: 10.1103/PhysRevE.82.026406 PACS number(s): 52.30.Cv, 47.65.−d, 47.27.Jv, 95.30.Qd

It is known that in the presence of a mean magnetic field assumed here to point in the z direction, $\mathbf{B}_0=B_0\hat{\mathbf{e}}_z$, nonlinear interactions in incompressible magnetohydrodynamics (MHD) are weakened in the field-parallel direction. The MHD approximation allows us to describe the large-scale dynamics of astrophysical plasmas, i.e., ionized gases, such as the interstellar medium or the solar corona. Due to the above-mentioned anisotropy, the nonlinear energy transfer in MHD turbulence proceeds preferably to larger perpendicular spatial wave numbers [1–4]. Direct numerical simulations show that the field-perpendicular energy spectrum exhibits self-similar inertial-range scaling in wave number $\sim k^{-m}$ with $m=5/3$ [5,6] for weak to moderate B_0, or $m=3/2$ [7–10] for strong B_0.

Iroshnikov [11] and Kraichnan [12] proposed the first theory of the effect of a mean magnetic field on incompressible MHD turbulence. They remarked that any flow can be decomposed into a sum of weakly interacting waves with different wave vectors k; the term "weak interaction" means that the characteristic time of deformation of the waves is much longer than their periods. This led to the prediction of a slow cascade, with a spectral slope $m=3/2$ different from the Kolmogorov prediction $m=5/3$.

This theory used an isotropic measure of the propagation time based on the modulus of the wave vector,

$$\langle \omega \rangle^{-1} = \langle (\mathbf{k}\cdot\mathbf{B}_0)^{-1} \rangle \simeq kB_0^{-1}, \tag{1}$$

ignoring deliberately the waves with wave vectors perpendicular (or almost perpendicular) to the mean field, for which the deformation time should clearly be smaller than their periods, and hence the interaction is strong. This was criticized by Goldreich and Sridhar [13], who denied the possibility of the previous weak cascade to occur and argued that the perpendicular strong cascade leading to $k_\perp^{-5/3}$ should be the only one present. For a large enough mean field, the perpendicular cascade should thus be restricted to a thin subset around the $k_\perp$ axis in Fourier space, with the subset becoming thinner when the mean field increases.

More precisely, the subdomain in $(k_\parallel, k_\perp)$ space where the perpendicular cascade is believed to occur is defined by a critical balance [13] between the characteristic time of nonlinear interaction, $\tau_{NL} \simeq (k_\perp u_\lambda)^{-1}$, and the Alfvén time $\tau_A \simeq (k_\parallel B_0)^{-1}$, with the fluctuations becoming correlated along the guide field up to a distance $\simeq B_0\tau_{NL}$, where u_λ is the typical magnitude of fluctuations at the scale $\lambda \simeq 1/k_\perp$. Assuming a scaling law in the perpendicular direction and spectral transfer dominated by strong coupling, i.e., $\chi=\tau_A/\tau_{NL} \gtrsim 1$, one obtains the three-dimensional (3D) spectrum

$$E_3(k_\parallel, k_\perp) = k_\perp^{-m-q-1} f(\chi), \tag{2}$$

where $\chi = k_0^{1-q} k_\perp^q k_\parallel^{-1} b_{\mathrm{rms}}/B_0$, with $m=5/3$ and $q=2/3$, $f(\chi) \simeq 1$ for $|\chi| \geq 1$ and $f(\chi)$ negligible for $|\chi| \ll 1$.

Equation (2) actually suffers from two limitations when the mean field B_0 is significantly larger than the magnetic fluctuation rms value. First, the spectral slope is observed to become $m=3/2$ [7–10] instead of the strong cascade value $m=5/3$; second, the time-scale ratio $\chi=\tau_A/\tau_{NL}$ becomes significantly smaller than unity [14] in the excited part of the spectrum, showing that the strict critical balance condition $\chi=1$ is too restrictive to describe the anisotropy of the cascade or, in other words, that the cascade is more extended in the oblique directions than predicted by the critical balance condition. This has led several authors to suggest modifications which either still assume that the anisotropy is dictated by the critical balance condition [15,16] or propose that the time-scale ratio χ decreases with increasing B_0 [17]. All

*roland.grappin@obspm.fr
†wolf.mueller@ipp.mpg.de

 ©2010 The American Physical Society

these phenomenologies predict a spectral form different from Eq. (2), with different spectral slopes in the perpendicular and parallel directions.

In the present paper, we analyze the angular spectrum and find by taking slices along the radial directions that a unique spectral form (and slope) holds in all directions, with the radial power-law range extent depending on the angle with the mean field. As a result, a significant portion of this spectrum lies in a domain where the time-scale ratio χ is subcritical, that is, much smaller than unity.

This study focuses on representative states of fully developed turbulence permeated by a strong mean magnetic field with $B_0=5b_{\rm rms}$ from high-resolution direct numerical simulations of quasistationary MHD turbulence forced at large scales. The forcing is realized by freezing all modes (velocity and magnetic field) with $k\leq 2$ in an energetically roughly isotropic and equipartitioned state. The driving of magnetic energy could be realized physically by large-scale fluctuations of electrical current, although here it is mainly applied to achieve a state of approximate equipartition of kinetic and magnetic energies. Decaying test simulations have confirmed that the forcing does not modify the results presented in the following. The dimensionless equations of resistive MHD formulated with the vorticity $\omega=\nabla\times\mathbf{v}$ and the magnetic field $\mathbf{b}$ are given by

$$\partial_t\omega=\nabla\times[\mathbf{v}\times\omega-\mathbf{b}\times(\nabla\times\mathbf{b})]+\mu\Delta\omega,$$

$$\partial_t\mathbf{b}=\nabla\times(\mathbf{v}\times\mathbf{b})+\eta\Delta\mathbf{b},$$

$$\nabla\cdot\mathbf{v}=\nabla\cdot\mathbf{b}=0.$$

The equations are solved by a standard pseudospectral method with spherical mode truncation to alleviate aliasing errors. The numerical resolution is $1024^2\times256$ collocations points with reduced resolution in the direction of $\mathbf{B}_0$ [8] and with kinematic viscosity μ and resistivity η set to $\mu=\eta=9\times10^{-5}$. The analyzed data are the temporal average of five snapshots of the three-dimensional Fourier energy distribution taken equidistantly within about four to five field-perpendicular large-scale turnover times $T_{0,\perp}$ of quasistationary turbulence where $T_{0,\gamma}=L_0/v_{\gamma\rm rms}=\pi/\langle v_\gamma^2\rangle^{3/2}\int d\mathbf{k}'\,\delta(k'_\gamma)|v_\gamma(\mathbf{k}')|^2$, with $\gamma\in\{x,y,z\}$ (cf. [18]) and $v_{\rm rms}\approx b_{\rm rms}=1$ with $T_{0,\perp}\approx1.5$ and $T_{0,\parallel}\approx1.7$. The normalized cross helicity $\rho=\langle\mathbf{v}\cdot\mathbf{b}\rangle/(\langle v^2\rangle^{1/2}\langle b^2\rangle^{1/2})$ and the Alfvén ratio $\langle v^2\rangle/\langle b^2\rangle$ fluctuate around 23% and 93%. The 3D-energy spectrum $E_3(k_x,k_y,k_z)$ relates to the total energy by $E^{\rm tot}=\int d^3x(v^2+b^2)/2=\int d^3kE_3(k_x,k_y,k_z)$.

Figure 1 shows contour levels of E_3 in two mutually orthogonal planes containing the origin. The field-perpendicular k_x-k_y plane [Fig. 1(a)] displays an isotropic energy distribution, as expected. Anisotropy induced by $\mathbf{B}_0$ appears in planes containing the B_0 direction [Fig. 1(b)].

Spectral anisotropy is traditionally diagnosed by one-dimensional (1D) spectra, e.g., $E_\perp(k_x)=\int d^3k'E_3\delta(|k_x|-k'_x)$ and $E_\parallel(k_z)=\int d^3k'E_3\delta(|k_z|-k'_z)$. These are shown compensated by $k^{3/2}$ [Fig. 2(a)] and by $k^{5/3}$ [Fig. 2(b)]. The perpendicular spectrum exhibits a power law with $m=3/2$, in agreement with previous works [7–10], while the parallel spectrum does not show any convincing scaling range. An

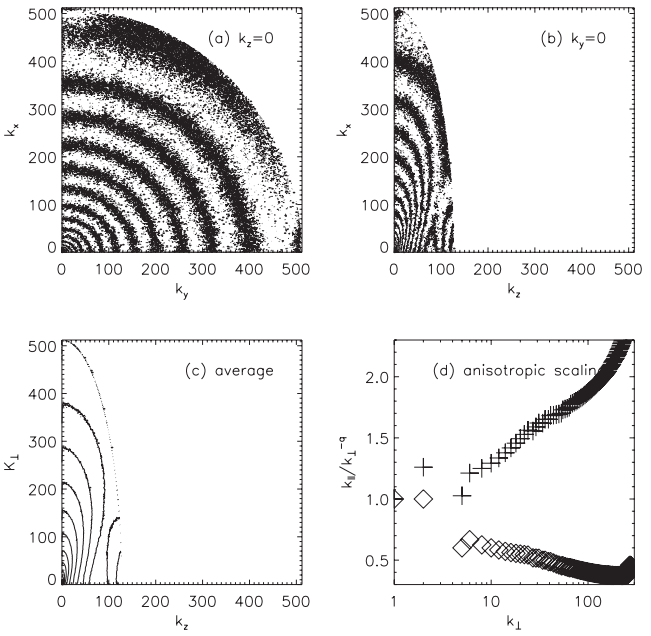

FIG. 1. Energy contour levels of three-dimensional spectral energy density $E_3(k_x,k_y,k_z)$: (a) plane $k_z=0$, (b) plane $k_y=0$, and (c) average of energy density over all planes containing $\mathbf{B}_0$. (d) Anisotropic scaling law between wave numbers $k_\perp$ and $k_\parallel$ (see text), with two compensated scalings: $k_\parallel(k_\perp)k_\perp^{-1}$ (diamonds) and $k_\parallel(k_\perp)k_\perp^{-2/3}$ (crosses).

anisotropic scaling law is build from the previous 1D spectra by plotting [Fig. 1(d)] the modes $(k_\perp,k_\parallel)$ sharing the same 1D energy density [14]. The anisotropy exponent q is seen to lie between $q=1$ and $q=2/3$, which is also obtained in [14] for $B_0=5$.

While planar integration yields some information about anisotropy, it mixes all wave numbers perpendicular to the chosen direction and thus blurs the separation between inertial and dissipative scales if the dissipative scale is not constant over the planar domain of integration. More importantly, no information on intermediate directions between parallel and perpendicular is available. Thus, spherical coordinates (k,θ,ϕ) with respect to the mean-field axis along $\hat{\mathbf{e}}_z$ are considered. As E_3 is isotropic in the azimuthal plane, the ϕ dependence of $E_3(k,\theta,\phi)$ is eliminated by averaging over $\phi\in[0,2\pi]$, which strongly decreases statistical noise

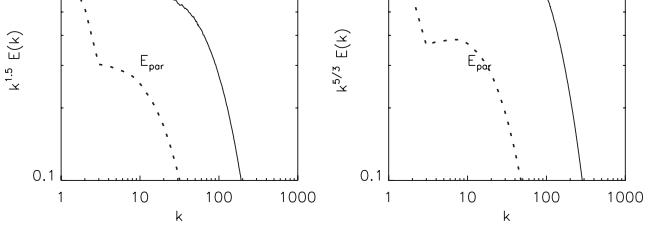

FIG. 2. Plane-integrated one-dimensional perpendicular and parallel energy spectra compensated by (a) $k^{3/2}$ and (b) $k^{5/3}$, respectively. The symbol k stands for the respective field-perpendicular and field-parallel wave numbers.

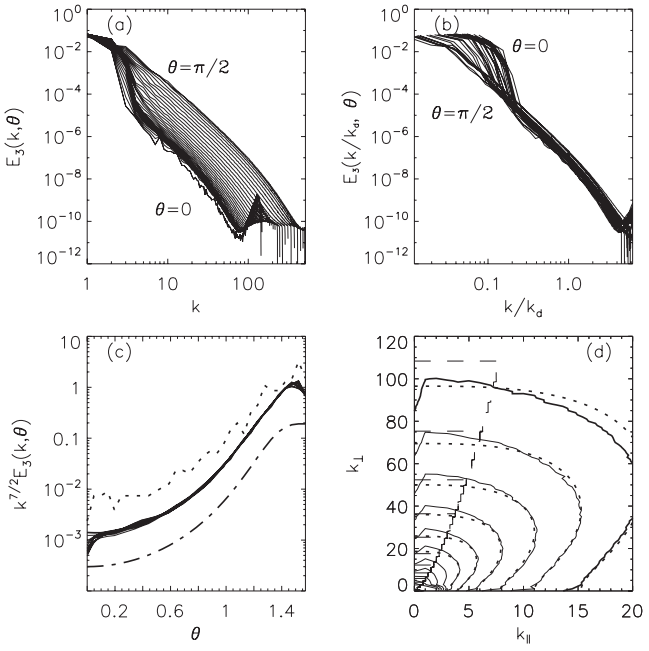

FIG. 3. Details of spectral properties: (a) $E_3(k,\theta)$ for θ ranging from 0 to $\pi/2$, (b) $E_3(k/k_d,\theta)$, (c) $k_d^{7/2}$ (dotted curve), $k^{7/2}E_3(k,\theta)$ for $8 \le k \le 20$ (solid curve), Eq. (7) with $m=3/2$ (dotted-dashed curve), and (d) energy contour levels of $E_3(k_\parallel,k_\perp)$: simulation data (solid); Eq. (2) (dashed line, with the oblique line tracing the boundary $\chi=1$ with $k_0=5$, $B_0=5$); Eqs. (3) and (7) with $\beta=3$, $\varepsilon=0.158$ (dotted curve).

and yields the ϕ-averaged 3D spectrum $E_3(k,\theta) = 1/(2\pi)\int d\phi E_3(k,\theta,\phi)$ whose isocontours in $(k_\parallel,k_\perp)$ are shown in Fig. 1(c). We define the corresponding 1D spectrum $E(k,\theta)$ as $E(k,\theta)=k^2E_3(k,\theta)$. The total energy is thus $E^{\rm tot}=2\pi\int k^2dk\int_0^{\pi/2}E_3(k,\theta)\sin(\theta)d\theta$.

The properties of $E_3(k,\theta)$ are shown in Fig. 3. A scaling range is seen starting at $k_0 \simeq 4-8$ down to a dissipative wave number $k_d(\theta)$. The 1D scaling exponent m

$$E_3(k,\theta) = A(\theta)k^{-m-2} \tag{3}$$

is *independent* of θ. The anisotropy appears at fixed k as a θ dependence of the spectral amplitude $A(\theta)$ and of the dissipative wave number $k_d(\theta)$. Normalizing the wave number by k_d shows that the spectrum follows a single functional form F whatever is θ:

$$E_3(k,\theta) = F(k/k_d) = F_0[k/k_d(\theta)]^{-m-2}, \tag{4}$$

where F_0 is a constant (the amplitude of the spectrum at the dissipative scale). Note that the first equality holds also beyond the dissipative range, with the second being valid for $k \le k_d$. A corollary is that

$$A(\theta) \propto k_d(\theta)^{m+2}. \tag{5}$$

Figure 3(a) shows the self-similar wave-number intervals of all $E_3(k,\theta)$ spectra, starting in the range $k_0 \simeq 4-8$ with a slight dependence on θ. The dissipative wave number $k_d(\theta)$ is estimated by locating the maximum of $k^2E(k)$ in each direction θ: varying θ from $\pi/2$ to 0 leads to a drop of $k_d(\theta)$ from about 100 to 14 while the spectral energy at fixed k decreases in the inertial range from 1 to 10^{-3}. Figure 3(b) indicates that the spectral θ dependence can be nearly eliminated by normalizing with k_d [Eq. (4)]. The relation between spectral amplitude $A(\theta)$ and $k_d(\theta)$ as given by Eq. (5) is confirmed in Fig. 3(c) which shows that $k_d^{7/2}$ (dotted curve) closely follows $A(\theta)=E_3(k,\theta)k^{7/2}$ [Eq. (3)], with $k \le 20$ to eliminate the dissipative range in the parallel direction.

A simple model of anisotropic spectrum with a spectral exponent being the same in all directions has been proposed previously in the context of shell models of turbulence [19] as well as solar wind turbulence [20,21]. It reads

$$A(\theta) = (\cos^2\theta/\varepsilon^2 + \sin^2\theta)^{-(1+m/2)}. \tag{6}$$

We tried to use this model to adjust the energy contours of our numerical simulations and found that the global anisotropy between the perpendicular and parallel amplitudes requires $\varepsilon=0.158$. However, the model fails to reproduce correctly the detailed angular anisotropy, that is, the contours in oblique directions, because our energy contours differ much from ellipsoids, as is seen in Fig. 3(d) which shows a zoom of the energy contours as solid curves [the model of Eq. (6) would produce circular contours in this figure]. However, we found that switching from 2 to 3 for the exponents of the sine and cosine as

$$A(\theta) = (\cos^3\theta/\varepsilon^2 + \sin^3\theta)^{-(1+m/2)} \tag{7}$$

leads to a reasonable good fit to the simulation results in all directions, as seen both in the dotted-dashed curve in Fig. 3(c) for the amplitude variation vs θ and in the dotted contours in the $(k_\parallel,k_\perp)$ plane in Fig. 3(d).

The energy contours of the critical balance spectrum [Eq. (2), with $B_0=5$ and $k_0=5$] are also represented by dashed lines in Fig. 3(d). They isolate a small cone about the $k_\parallel$ axis in the whole plane, so excluding a large part of the angular structure of the true angular spectrum. Note that the dissipative wave number is determined up to an error of about a factor of 2 (due to errors in interpolating the spectrum), which leads to the noisy appearance of the curve of k_d in Fig. 3(c), to the finite thickness of the normalized spectra in Fig. 3(b), and to variations of about a factor of 4 in the constant F_0 in Eq. (4).

To determine the scaling exponent m of $E(k,\theta) \sim k^{-m}$, the 1D spectra averaged over four θ intervals and compensated by $k^{3/2}$ and $k^{5/3}$ are shown in Fig. 4. The spectrum with $\theta=\pi/2$ is represented by the bold line. The $m=3/2$ scaling is seen to be dominant, except possibly for group B which follows $m=5/3$ [Fig. 4(a)]. The extent of the 3/2 inertial range is shown by oblique dashed lines; it is bounded on the right by k_d and on the left by an intermediate range which separates the inertial from the forcing range. The start of the inertial range is thus growing from $k \simeq 5$ to 10 for $\theta \to \pi/2$.

Increasing the mean field up to $B_0=5\sqrt{2}$ in test simulations (not shown) leads to further decrease in the power-law range in the parallel direction, with the perpendicular range increasing slightly and the parallel range decreasing substantially, so that the ratio of both ranges varies with B_0 as

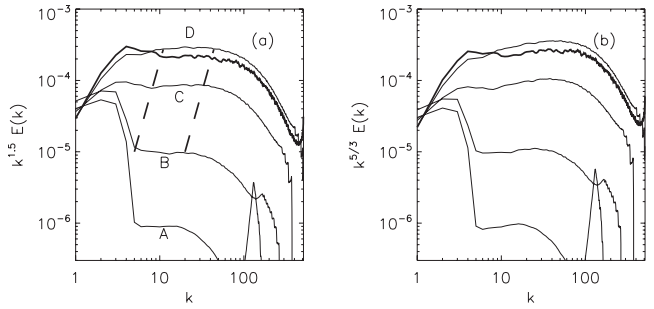

FIG. 4. Spectra averaged in four subsets of directions. A, $14° \le \theta \le 39°$; B, $42° \le \theta \le 65°$; C, $67° \le \theta \le 76°$; D, $79° \le \theta \le 90°$; direction $\theta = 90°$ as thick curve. (a) Spectra compensated by $k^{3/2}$, with the two oblique dashed lines indicating roughly the inertial range; (b) spectra compensated by $k^{5/3}$.

$$k_d(\pi/2)/k_d(0) = [A(\pi/2)/A(0)]^{1/(m+2)} \simeq B_0. \tag{8}$$

Note that the fit by Eq. (7) remains as good as in Fig. 3(d) after decreasing ε by a factor of $\sqrt{2}$, as expected since Eq. (7) implies $k_d(\pi/2)/k_d(0) = 1/\varepsilon$; hence, from Eq. (8), $\varepsilon \simeq 1/B_0$. Increasing again B_0 up to 10 confirmed this trend, but the parallel range becomes too small in that case to allow a good determination of the associated dissipative wave number. This precludes checking that the spectrum normalized by k_d is angle independent for small θ. This difficulty could be alleviated by increasing the numerical resolution which would allow increasing the Reynolds number. We choose instead below to compare with ideal MHD simulations with 512^3 resolution and with $B_0 = 5$ and 10.

In the ideal case, Fourier space is divided in a large-scale range, presenting spectral properties close to those of a standard turbulent spectrum with dissipation, and a small-scale range where the spectral slope increases, with the latter scales playing the role of a dissipative range (cf. [22] in the hydrodynamic case). The boundary between the two domains slowly shifts with time to ever larger scales. It can be identified with the dissipative wave number, thus determined here as the minimum of the 1D spectrum. The simulations are initialized with a quasistationary state of the resistive run and are continued without any dissipation and with the chosen B_0 in the same numerical setup until the energetically rising small scales begin to pollute the scaling region. Choosing the appropriate time, power-law ranges in all directions can be properly identified even with a large field $B_0 = 10$. The resulting power law is now found to be $m = 5/3$ both with $B_0 = 5$ and 10, contrary to the resistive runs. This difference in scaling between the resistive and ideal runs might be attributed to a different role played by the bottleneck effect [23] in these two setups. All reported findings [cf. Eqs. (3)–(8)] are however confirmed when setting $m = 5/3$, as seen in Fig. 5 which shows the anisotropy in two ideal runs with $B_0 = 5$ and $B_0 = 10$.

Let us go back to the resistive case. As already found in [14], we find that the excited part of the $k_\parallel, k_\perp$ space is not restricted to regions where $\chi \ge 1$. The important point is that the 3D-energy contours, and as well the boundary of the power-law range, ignore the isocontours of χ as shown in

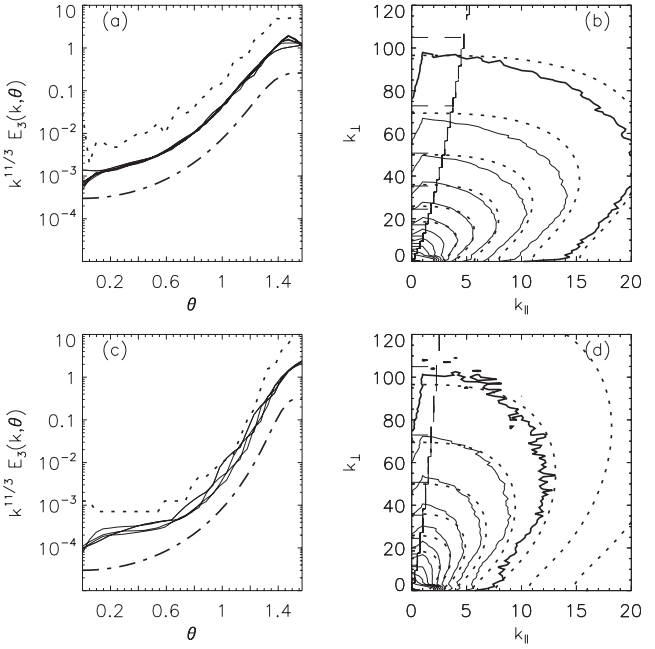

FIG. 5. Anisotropy in ideal runs: (a) and (b) $B_0 = 5$ and (c) and (d) $B_0 = 10$. (a)–(c) $k_d^{11/3}$ (dotted curve), $k^{11/3}E_3(k,\theta)$ (solid curve) (a) for $6 \le k \le 12$ and (b) for $5 \le k \le 8$, Eq. (7) (dashed-dotted curve) with $m = 5/3$, and (a) $\varepsilon = 0.158$ and (c) $\varepsilon = 0.158/2$. (b)–(d) Energy contour levels of $E_3(k_\parallel, k_\perp)$: simulation data (solid curve); Eq. (2) [dashed line, with the oblique line tracing the boundary $\chi = 1$ with $k_0 = 5$ and (b) $B_0 = 5$ and (d) $B_0 = 10$]; Eqs. (3) and (7) with $\beta = 3$ and (b) $\varepsilon = 0.158$ and (d) $\varepsilon = 0.158/2$ (dotted curve).

Fig. 3 [see also Figs. 5(b) and 5(d)]: the form of the 3D-energy contours, as well as the angle-independent spectral slope, actually suggests an isotropic cascade, that is, a cascade along radial directions. To test this idea, we define a θ-dependent effective Reynolds number $\mathrm{Re}_0 \propto A(\theta)^{1/2}$ based on the energy density $A(\theta)k_0^{-m-2}$ at k_0. For $\theta = 0 \to \pi/2$, Re_0 increases by a factor of 30, while k_d grows by a factor of 10, as

$$k_d \propto \mathrm{Re}_0^{\alpha}, \tag{9}$$

where $\alpha = 2/(m+2) \simeq 1/2$, with m being the 1D slope. The exponent in Eq. (9) is substantially smaller than the value $\alpha = 3/4$ for $m = 5/3$ [or 2/3 in the case $m = 3/2$] obtained by equating the input flux at k_0 and the dissipative flux $\epsilon \simeq \nu k_d^2 u(k_d)^2$. This means that if θ increases from zero to $\pi/2$, the inertial range increases more slowly than it would if the dissipative loss at small scales would balance the input energy rate at the ($k_0 \simeq 8$) wave number which marks the large-scale boundary of the inertial range. Hence, for $\theta \to \pi/2$ the nonlinear radial energy flux must be depleted while the contrary is true for the parallel directions.

By examining the solar wind turbulence, it has been shown [20] that the power-law index of the fluctuation spectra is independent of the angle between the wave vector and the mean interplanetary magnetic field, which is fully compatible with the results reported here from direct simulations. Other studies of solar wind turbulence have however reached a different conclusion [24]. The latter study used wavelet

transforms, which allows to define parallel and perpendicular directions with respect to local averages of the magnetic field. Indeed, it has been argued in [5,6] that the critical balance phenomenon and the associated spectral laws (in particular the anisotropy index $q=2/3$ relating the perpendicular and parallel wave numbers) emerge only when considering, instead the mean field, the local average field. In the work by Bigot *et al.* [14] who considered as we do only the global mean field, the $q=2/3$ law appears clearly only when the mean field is large enough, which can be explained by the fact that in this limit the local and mean-field approaches coincide. According to this viewpoint, the results reported here should be a simple artifact of the fact that our frame is not attached to the local mean field, but to the global mean field.

However, while the effect could indeed appear for interplanetary turbulence where the fluctuation level is high, it is hardly the case here since $B_0/b_{\mathrm{rms}}=5$ or 10. Besides, it is remarkable that the fit by our anisotropy function in Fig. 5 when $B_0=5b_{\mathrm{rms}}$ is as good as when $B_0=10b_{\mathrm{rms}}$, which is an indication that the spectral properties of the turbulence are correctly revealed by using our method.

A possible way to reconcile both pictures is the following. It takes into account the fact that there is a second parameter, the Reynolds number. Indeed, as the anisotropy increases with B_0, we find that the scaling range in the parallel direction decreases accordingly [Eq. (8)], which implies that, at a fixed viscosity, the parallel power-law range disappears at even moderate B_0. In our case, $k_{d\perp}\simeq 100$ and $k_{d\parallel}\simeq 10$ when $B_0=5b_{\mathrm{rms}}$, while the start of the scaling range is $k_0\simeq 5-8$, preventing to increase significantly B_0. The regime at high B_0 will thus depend on the Reynolds number (Re). Increasing B_0 at fixed perpendicular Re depletes the field-parallel cascade and could ultimately lead to critically balanced turbulence. If B_0 and Re are however large enough, e.g., under astrophysical conditions, allowing for scaling in all directions, then the properties described in this work are expected to hold. We thus propose direction-independent scaling for high Re and critically balanced turbulence at low Re. The crossover Re value is expected to increase with B_0. A strong indication in this sense is found in [14] where the anisotropy scaling exponent q is seen to be between 1 and 2/3 at $B_0=5b_{\mathrm{rms}}$ as in here [Fig. 1(d)], while it begins to cluster around 2/3 at $B_0/b_{\mathrm{rms}}\geq 10$. Such a good agreement with $q=2/3$ is found already at $B_0/b_{\mathrm{rms}}\simeq 1$ in [5] because of a moderate Reynolds number.

We have reported here two previously unknown properties of the MHD angular energy spectra: (i) its functional form is $A(\theta)f(k)$ and (ii) the anisotropy function $A(\theta)$ is best expressed [Eq. (8)] as the ratio of the perpendicular over the parallel power-law range extent, which scales linearly with B_0 in the $B_0/b_{\mathrm{rms}}=5,10$ interval considered here. These results offer important tests for future theories of anisotropic turbulence.

We thank G. Belmont, J. Léorat, and A. Busse for several fruitful discussions.

[1] H. R. Strauss, Phys. Fluids **19**, 134 (1976).
[2] D. Montgomery and L. Turner, Phys. Fluids **24**, 825 (1981).
[3] J. V. Shebalin, W. H. Matthaeus, and D. Montgomery, J. Plasma Phys. **29**, 525 (1983).
[4] R. Grappin, Phys. Fluids **29**, 2433 (1986).
[5] J. Cho and E. T. Vishniac, Astrophys. J. **539**, 273 (2000).
[6] J. Cho, A. Lazarian, and E. T. Vishniac, Astrophys. J. **564**, 291 (2002).
[7] J. Maron and P. Goldreich, Astrophys. J. **554**, 1175 (2001).
[8] W.-C. Müller and R. Grappin, Phys. Rev. Lett. **95**, 114502 (2005).
[9] P. D. Mininni and A. Pouquet, Phys. Rev. Lett. **99**, 254502 (2007).
[10] J. Mason, F. Cattaneo, and S. Boldyrev, Phys. Rev. E **77**, 036403 (2008).
[11] P. S. Iroshnikov, Astron. Zh. **40**, 742 (1963).
[12] R. H. Kraichnan, Phys. Fluids **8**, 1385 (1965).
[13] P. Goldreich and S. Sridhar, Astrophys. J. **438**, 763 (1995).
[14] B. Bigot, S. Galtier, and H. Politano, Phys. Rev. E **78**, 066301 (2008).
[15] S. Boldyrev, Phys. Rev. Lett. **96**, 115002 (2006).
[16] G. Gogoberidze, Phys. Plasmas **14**, 022304 (2007).
[17] S. Galtier, A. Pouquet, and A. Mangeney, Phys. Plasmas **12**, 092310 (2005).
[18] O. Zikanov and A. Thess, Appl. Math. Model. **28**, 1 (2004).
[19] V. Carbone and P. Veltri, Geophys. Astrophys. Fluid Dyn. **52**, 153 (1990).
[20] J. A. Tessein, C. W. Smith, B. T. MacBride, W. H. Matthaeus, M. A. Forman, and J. E. Borovsky, Astrophys. J. **692**, 684 (2009).
[21] V. Carbone, F. Malara, and P. Veltri, J. Geophys. Res. **100**, 1763 (1995).
[22] C. Cichowlas, P. Bonaïti, F. Debbasch, and M. Brachet, Phys. Rev. Lett. **95**, 264502 (2005).
[23] A. Beresnyak and A. Lazarian, e-print arXiv:1002.2428.
[24] T. S. Horbury, M. Forman, and S. Oughton, Phys. Rev. Lett. **101**, 175005 (2008).